Available online at www.sciencedirect.com
ScienceDirect
Trans. Nonferrous Met. Soc. China 22(2012) 2191−2197
Transactions of Nonferrous Metals Society of China
www.tnmsc.cn

A Cu-based bulk amorphous alloy composite reinforced by carbon nanotube

CAI An-hui[1, 2], XIONG Xiang[2], LIU Yong[2], AN Wei-ke[1], ZHOU Guo-jun[1], LUO Yun[1], LI Tie-lin[1], LI Xiao-song[1]

1. College of Mechanical Engineering, Hunan Institute of Science and Technology, Yueyang 414006, China;
2. State Key Laboratory of Powder Metallurgy, Central South University, Changsha 410083, China

Received 26 September 2011; accepted 11 February 2012

Abstract: Bulk $Cu_{50}Zr_{40}Ti_{10}$ amorphous alloy composites reinforced with carbon nanotube (CNT) were successfully fabricated by hot pressing technique. Their density, thermal conductivity, and mechanical properties were systemically investigated. The density and the compression strength of the compacts both decrease with increasing CNT content. The thermal conductivity of the compacts decreases when the CNT content is less than 0.10% or exceeds 0.60% (mass fraction), while increases when the CNT content is in the range of 0.1%−0.6%. The strain limit and the modulus of the compacts are obviously improved when the CNT content is less than 1.0% and then decrease significantly when the CNT content exceeds 1.00%. The optimum CNT addition is less than 0.20% at the comprehensive properties point of view.

Key words: Cu-based amorphous alloy; carbon nanotube; composite

1 Introduction

Bulk amorphous alloys (BAAs), with many unique properties, such as excellent corrosion resistance, remarkably high strength and hardness and large elastic deformation limit [1,2], usually show little overall room temperature plasticity due to the formation of highly localized shear bands resulting in a catastrophic failure. Attempts have been made to enhance the ductility of BAAs by introducing crystalline phase [3], adding particles and/or fibres [4−9], in situ formed ductile phase precipitates [10−13], and by producing porous/foam BAAs during casting or consolidation process [8,14,15]. However, the BAA composites by casting technique exhibit limitations on controlling the volume fraction and particle size of the reinforcements. The glass forming ability is also affected by the chemical reactions between second phase and melt during casting process as for the BAA composites by introducing second phase (particle and/or fibre), resulting in the difficult formation of these BAA composites [16,17].

Powder metallurgy techniques can be easily applied to preparing amorphous composites and to overcoming the above mentioned restrictions. Recently, BAA composites are synthesized by consolidation of amorphous composite powders using a viscous flow of the amorphous powders in the supercooled liquid region $\Delta T_x=T_x-T_g$ (T_x and T_g are the onset crystallization temperature and glass transition temperature, respectively) [4−9,18−21]. The more the T_x is, the easier the realization of the temperature control during the consolidation of the amorphous alloy powders.

It is known that Cu−Zr−Ti alloy is a good glass former and exhibits high a mechanical strength and a high thermal stability. $Cu_{50}Zr_{40}Ti_{10}$ amorphous alloy [22] characterizes in high tensile fracture strength, low elastic modulus, and good corrosion behavior. On the other hand, the $Cu_{50}Zr_{40}Ti_{10}$ amorphous alloy presents high ΔT_x (66.7 K [22]). Its hardness is the lowest in $Cu_{50+x}Zr_{40-x}Ti_{10}$ alloy system [23]. These results indicate that the $Cu_{50}Zr_{40}Ti_{10}$ amorphous alloy would be suitable for the hot pressing. Moreover, the T_g of the $Cu_{50}Zr_{40}Ti_{10}$ amorphous alloy is 624.4 K [22], indicating its low-temperature consolidation capacity.

The thermal conductivity of the amorphous alloys is needed to calculate cooling rates during the synthesis of BAAs and also to estimate local heating associated with

Foundation item: Project (50874045) supported by the National Natural Science Foundation of China; Projects (200902472, 20080431021) supported by the China Postdoctoral Science Foundation; Project (10A044) supported by the Research Foundation of Education Bureau of Hunan Province of China

Corresponding author: CAI An-hui; Tel: +86-730-8648848; E-mail: cah1970@sohu.com

DOI: 10.1016/S1003-6326(11)61448-9

narrow shear instability during plastic deformation. In addition, their thermophysical properties are useful for studies of practical applications such as welding and machining, in order to determine the optimum conditions for welding and/or machining BAAs without crystallization [24,25], while the work on the thermal-physical properties is scarce [26−29].

On the other hand, the carbon nanotube (CNT) has been extensively used in many fields [30,31] due to its high aspect ratio, high mechanical property, high electrical and thermal conductivity, and high chemical and thermal stability, respectively [32,33]. It has been investigated to obtain the composites by adding the organic or inorganic materials [16,17,34−37]. However, the BAA composites reinforced by the carbon nanotube were scarcely investigated [16,17,38].

In the present work, we report the formation of a Cu-based BAA composite reinforced by the CNT using hot pressing technique without vacuum and inert gas protection. The thermal and mechanical properties of the Cu-based BAA composites were systematically investigated.

2 Experimental

2.1 Experimental procedures

Master ingots of the $Cu_{50}Zr_{40}Ti_{10}$ alloy (composition is given in nominal mole fraction) were prepared by arc melting a mixture of high purity Cu, Zr and Ti in a Ti-gettered argon atmosphere. The $Cu_{50}Zr_{40}Ti_{10}$ glassy alloy powders were produced by a high pressure argon gas atomization method. Atomization of the $Cu_{50}Zr_{40}Ti_{10}$ alloy was carried out in a closely coupled nozzle atomizing system. The master alloy was induction heated at 1200 K in an alumina crucible under a vacuum of 10^{-2} Pa. The melt was teemed through a guide tube, and atomized by a jet of Ar at 4.0 MPa. The $Cu_{50}Zr_{40}Ti_{10}$ powder was collected and sieved in a closed system filled with inert gas. After the mixing of the $Cu_{50}Zr_{40}Ti_{10}$ powders and multi-wall carbon nanotubes (MWCNT, outside diameter>50 nm, length~20 um, and purity>95%), a uniaxial pressing method was conducted using top and bottom stainless steel punches. In order to alleviate the oxidation of the powders, the powders were pre-compacted at pressure of 150 MPa before hot pressing. Then the powders were hot pressed at the temperature of 380 °C under the pressure of 450 MPa for 30 s. The hot pressed specimens were in cylindrical shape of d10 mm×5 mm for the thermal conductivity measurement and of d10 mm×20 mm for the compressive test, respectively.

2.2 Testing methods

The size of the gas-atomized powder was measured by a size analyzer. The structures of the powder, carbon nanotube (CNT), and bulk samples were examined by X-ray diffractometry (XRD) in reflection with a monochromatic Cu K_α radiation. The thermal stability of the as-atomized powder was examined by differential scanning calorimetry (DSC) at a heating rate of 0.5 K/s. The density of the consolidated specimens was determined by an Archimedean method. The thermal diffusivity was measured using a laser flash method. The thermal conductivity (κ, W/(m·K)) was calculated by an equation of $\kappa=\alpha\rho c_p$, where α, ρ and c_p are thermal diffusivity, bulk density, and specific heat capacity, respectively. The mechanical property under uniaxial compression was measured using a mechanical testing machine at a strain rate of 5×10^{-2} s^{-1}. The microstructure was characterized by scanning electron microscopy (SEM). The experimental results are shown in Table 1.

Table 1 Properties of $Cu_{50}Zr_{40}Ti_{10}$ BAA composites reinforced by carbon nanotube (CNT)

Content of CNT/%	Density/ ($g\cdot cm^{-3}$)	Thermal conductivity/ ($W\cdot m^{-1}\cdot K^{-1}$)	Compression strength/MPa	Strain limit/%
0	7.05	3.85	1181.0	6.7
0.05	6.83	3.30	1057.0	10.0
0.10	6.75	2.78	889.2	9.1
0.20	6.71	2.98	813.6	9.0
0.30	6.64	2.94	749.0	9.2
0.40	6.59	3.16	697.7	8.6
0.50	6.52	3.22	641.3	9.2
0.60	6.50	3.32	597.1	8.9
0.70	6.45	2.85	547.8	8.7
0.80	6.42	2.75	354.9	6.9
1.00	6.40	2.15	280.3	2.1
1.50	6.30	2.15	236.8	2.9

3 Results

The average size of the gas-atomized powder is 42.5 μm according to the results of size analysis. The SEM morphology of the gas-atomized $Cu_{50}Zr_{40}Ti_{10}$ powder is shown in Fig. 1. Most of the gas-atomized powders are in spherical form and which can be suitable for the consolidation of powder by hot pressing.

The formation of amorphous phase of the gas-atomized $Cu_{50}Zr_{40}Ti_{10}$ powder was confirmed by XRD. The XRD pattern of the gas-atomized powder is shown in Fig. 2. As can be seen in Fig. 2, fully amorphous phase of the gas-atomized powder is formed in the average particle size range below 42.5 μm. Therefore, the $Cu_{50}Zr_{40}Ti_{10}$ amorphous powders with the average particle size of 42.5 μm were used for subsequent consolidation in this study.

The thermal stability and crystallization behavior of the $Cu_{50}Zr_{40}Ti_{10}$ amorphous powder were examined by DSC measurement. Figure 3 shows the DSC curve of the $Cu_{50}Zr_{40}Ti_{10}$ amorphous powder at a constant heating rate of 0.5 K/s. As shown in Fig. 3, the onset temperature of crystallization (T_x) is 693.2 K. Below the onset of crystallization, the glass transition (T_g), which is shown as an endothermic reaction in the DSC curve, occurs at 629.5 K. This means that a fairly large supercooled liquid region ΔT_x of 63.7 K exists for gas-atomized $Cu_{50}Zr_{40}Ti_{10}$ amorphous powder, which is slightly lower than the literature data measured with melt spun $Cu_{50}Zr_{40}Ti_{10}$ amorphous ribbons [22].

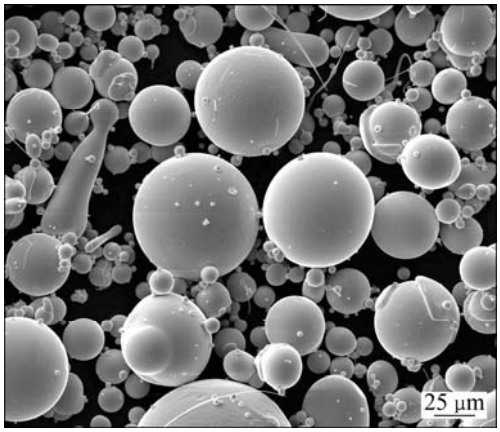

Fig. 1 SEM image of gas-atomized $Cu_{50}Zr_{40}Ti_{10}$ powder

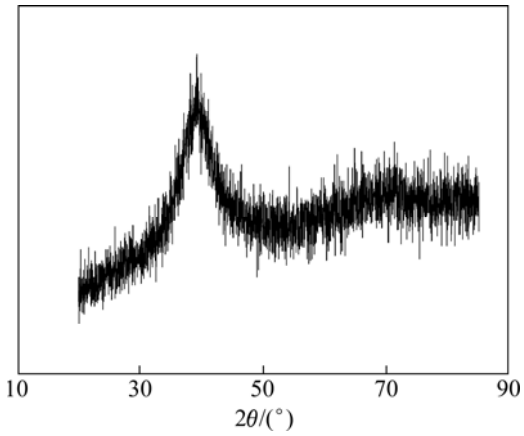

Fig. 2 X-ray diffraction pattern of gas-atomized powder

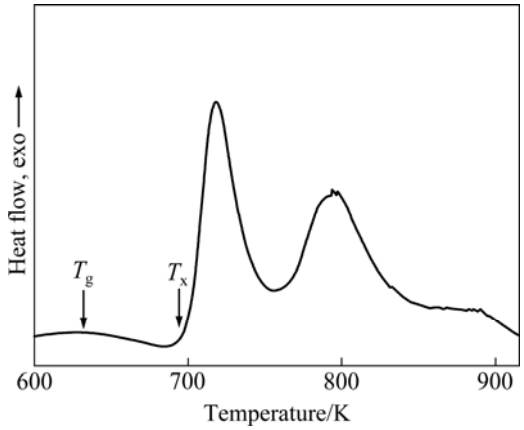

Fig. 3 DSC curve of $Cu_{50}Zr_{40}Ti_{10}$ amorphous powder at constant heating rate of 0.5 K/s

Figure 4 presents the XRD patterns of the CNT and the consolidated specimens with different CNTs. It is clearly seen from Fig. 4 that the XRD patterns of the consolidated specimens show sharp peaks belonging to CuO and ZrO_2 superimposed on a broad halo peak, indicating that the consolidated specimens are all somewhat oxidized. The consolidated specimens are oxidized more and more seriously when the CNT content is less than 0.30% or exceeds 0.70%, because the intensity of the peaks increases in these regions. However, the oxidation of the specimens is relieved when the CNT content is between 0.30% and 0.70%.

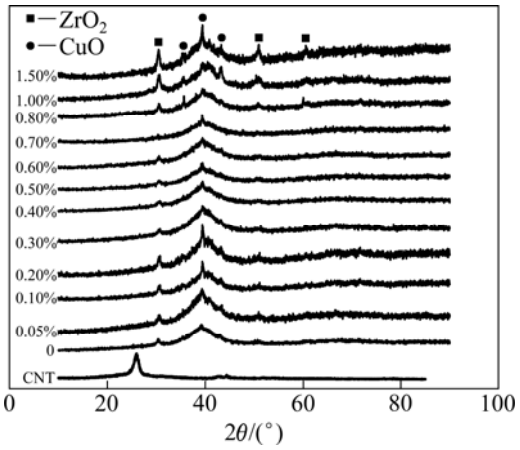

Fig. 4 XRD patterns of carbon nanotube (CNT) and consolidated specimens with different CNTs

The density and thermal conductivity of the consolidated specimens were measured by the Archimedean method and laser flash method, respectively. Two parameters are listed in Table 1 and the changes of two parameters with the CNT content are presented in Fig. 5. As shown in Table 1 and Fig. 5, the density of the consolidated specimen decreases with increasing CNT content. The thermal conductivity of the consolidated specimens continuously decreases when the CNT content is less than 0.10% and exceeds 0.60%, respectively, and increases when the CNT content is between 0.1% and 0.6%.

The mechanical properties of the consolidation specimens were measured by uniaxial compression test at a strain rate of 5×10^{-2} s^{-1}. The compressive stress—strain curves are plotted in Fig. 6. As shown in Fig. 6, the slopes of the stress — strain curves for the BAA composites with <1.0% CNT are smaller than those of monolithic BAA, indicating that the toughness of the BAA composite can be improved by the CNT addition.

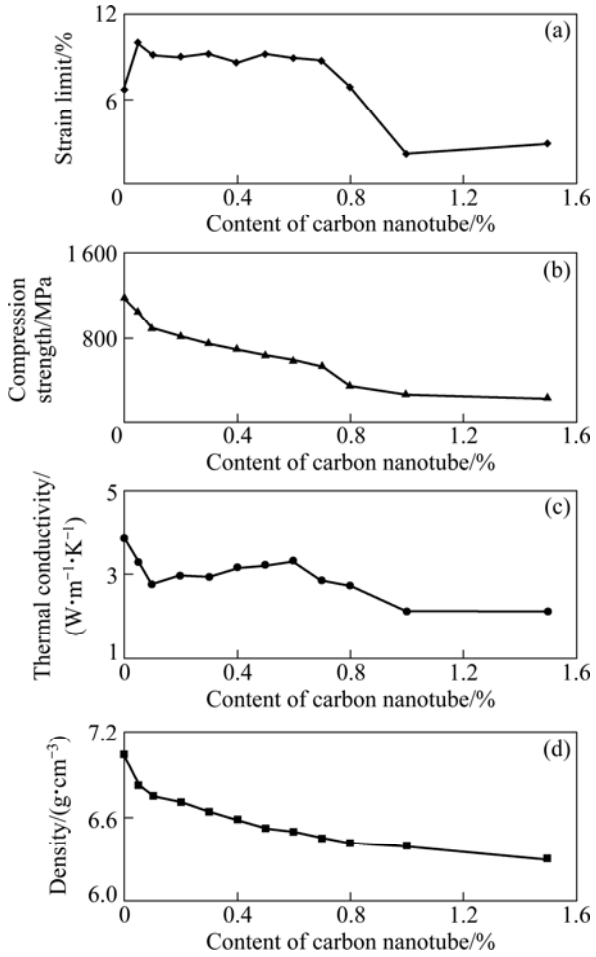

Fig. 5 Relationships between properties and CNT content for consolidated specimens (The line is used to guide the eye)

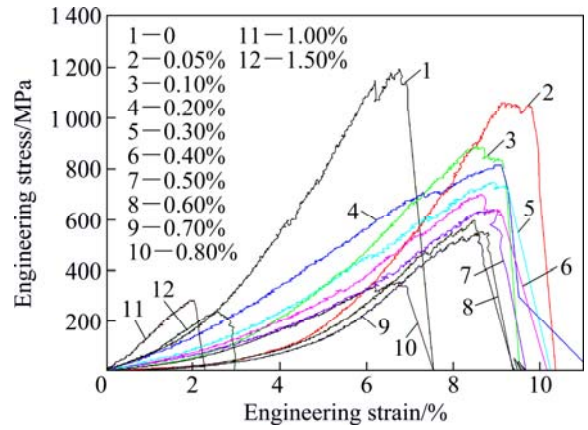

Fig. 6 Compressive stress—strain curves of consolidated specimens with different CNTs

When the CNT content exceeds 1.0%, the slopes of the stress—strain curves of the BAA composites are larger than those of the monolithic BAA. In addition, the mechanical properties are listed in Table 1 and the changes of the mechanical properties with the CNT content are presented in Fig. 5. As shown in Table 1 and Fig. 5, the compression strength of the specimen decreases with increasing CNT, indicating that the CNT is disadvantageous for improvement of the strength. In addition, the strain limit of the BAA composite is improved by the CNT addition when the CNT content is less than 0.80%. However, the strain limit of the BAA composites is less than that of the monolithic BAA when the CNT content exceeds 0.80%.

In order to investigate the effect of introducing CNT in the amorphous matrix on the fracture behavior, fracture surface of the failed compacts was observed by using SEM. The SEM micrographs of the compressive fracture surfaces with different CNT contents are shown in Fig. 7. As shown in Fig. 7(a), the fracture surface of

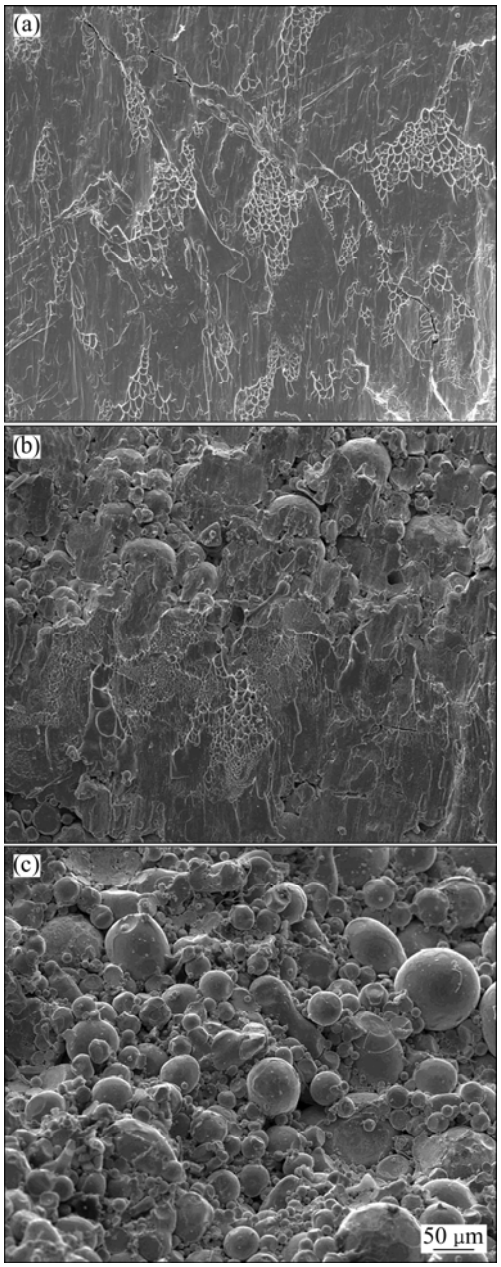

Fig. 7 SEM images of consolidated specimens containing different carbon nanotubes: (a) Without CNT; (b) 0.005%−0.8% CNT; (c) 1.0%−1.5% CNT

the monolithic BAA shows the classic vein-like fracture pattern and some cracks propagate along powder boundaries. As for the BAA composites containing 0.05%−0.8% CNT, the fracture surface shows the classic vein-like and smooth cleavage fracture patterns as well as the fracture along particle boundaries. In addition, there are many pores between the amorphous alloy powders and the cracks initiate and propagate along particle boundaries. When the CNT content exceeds 0.8%, most of amorphous powders present original spherical form, indicating the deterioration of the deformability of the amorphous powders by the CNT addition. Thus, the compacts containing 1.00% and 1.50% CNT fracture along power boundaries.

4 Discussion

As shown in Fig. 4, the compacts are all somewhat oxidized, and the oxidized degree of the consolidated specimens is not relieved with increasing CNT content. The oxidation of the specimens would be due to not only the residual oxidizing gas in the holes among the powders but also the absorbed oxidizing gas on the inner and exterior surface of the CNT. The holes are partially filled by the CNT, resulting in the decrease of the content of the residual oxidizing gas. While the absorbed oxidizing gas increases with increasing CNT content. Thus, the specimens are oxidized more and more seriously with increasing CNT content when the CNT content is less than 0.30%. In addition, the oxidizing degree of the specimens increases when the CNT content exceeds 0.70%. It would be due to the increase of the absorbed oxidizing gas as well as the increase of the holes resulted from the agglomeration of the CNT (see Fig. 8), although most of the holes are filled by the CNT. Nevertheless, when the CNT content is between 0.30% and 0.70%, the oxidized degrees of the specimens is the fact relieved with increasing CNT content. It would be due to that the holes are effectively filled by the CNTs in spite of the increase of the content of the absorbed oxidizing gas. In addition, these results would be also related to the pre-performing pressure in this study. The pre-performing pressure of 150 MPa would be somewhat low for densification of the green pressing as possible. The more the CNT content is, the lower the green density of the green pressing is.

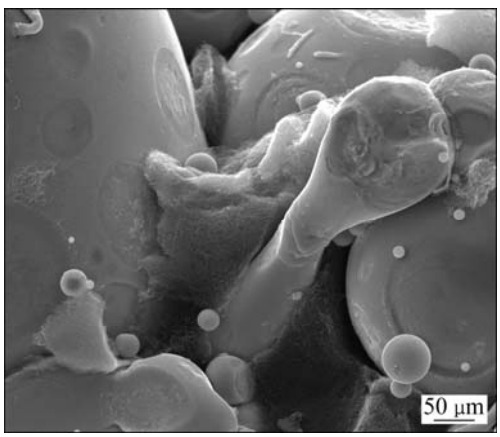

Fig. 8 Typical SEM morphology of distribution of carbon nanotube in consolidated specimens

The densities of the compacts decrease with increasing CNT content as shown in Table 1 and Fig. 5. It is due to the increase of the holes, as shown in Fig. 7 and Fig. 8. It is well known that the plastic deformation capacity of the CNT is worse than that of the amorphous alloy when the amorphous alloy is in the supercooled liquid region. Thus the adhesion between the CNTs is mainly mechanical. In addition, it is clearly seen from Fig. 7 and Fig. 8 that the addition of the CNT influences the deformation of the amorphous alloy powder because the magnitude of prior amorphous powder is more and more with increasing CNT content. On the other hand, it is clearly seen from Fig. 4 that the compacts are partially oxidized and the oxides are composed of CuO and ZrO_2. These hard and brittle oxides would deteriorate the consolidation capacity of the amorphous powders. Finally, the flow ability of the partially oxidized amorphous alloy powders is not enough high at 380 °C far away from the onset crystallization temperature 420 °C because the viscosity of the supercooled liquid decreases with increasing temperature in supercooled liquid region. And it would be that the pressure of 450 MPa for hot pressing is somewhat low for further densification of the samples.

As shown in Table 1 and Fig. 5, the thermal conductivity of the compacts decreases when the CNT is less than 0.10% and exceeds 0.60%, respectively. According to the solid-state physics, the thermal conductivity of the metal or alloy depends on the transmission of the electron and the phonon, which is related to the defects, such as the holes, interfaces and particle boundaries, in the material. The more the defects are, the stronger the scattering of the electron and the phonon are resulting in the decrease of the thermal conductivity. As shown in Table 1, the density of the compacts decreases with increasing CNT content, indicating the increase of the holes. In addition, the magnitude of the powder boundary increases with increasing CNT content, as shown in Fig. 7. As shown in Fig. 4, the compacts are partially oxidized, resulting in the increase of the magnitude of the interfaces. These results are disadvantageous for the transmission of the electron and phonon, although the increase of the CNT can improve the thermal conductivity. However, the

thermal conductivity increases when the CNT content is between 0.10% and 0.60%. It would result from the reason that the decrease of the oxide content and the increase of the CNT play a more important role than the decrease of the defects.

As shown in Table 1 and Ref. [22], the compression strength of the consolidated monolithic $Cu_{50}Zr_{40}Ti_{10}$ BAA is lower than the tensile strength of the $Cu_{50}Zr_{40}Ti_{10}$ amorphous ribbon, while the strain limit of the former is larger than that of the latter. It would be due to the continuity and homogeneity of materials. Generally, the as-spun amorphous alloy ribbon is continuous and homogeneous, resulting in a catastrophic failure. However, the consolidated BAA is composed of many powders with different sizes, resulting in many powder boundaries. In addition, the $Cu_{50}Zr_{40}Ti_{10}$ amorphous powder is oxidized during the hot-pressing procedure (see Fig. 4), resulting in an oxide film on the powder. Therefore, the bond strength of the powders is largely deteriorated, resulting in the decrease of the compression strength of the consolidated BAA. On the other hand, the slip can be set out along the powder boundary (see Fig. 7(a)), resulting in the increase of the strain limit and the decrease of the compression strength of the consolidated BAA.

The compression strength of the compacts decreases with increasing CNT content, as shown in Fig. 5 and Table 1. It would be due to the fact that: 1) the decrease of the density (Table 1 and Fig. 5) reduces the loaded area; 2) the increase of the magnitude of the powder boundary and the interface (Fig. 7) results in the increase of the magnitude of the defects for the origination and the propagation of the cracks (Fig. 7).

As shown in Fig. 6, the $Cu_{50}Zr_{40}Ti_{10}$ BAA composites characterize in higher strain limit than the monolithic BAA when the CNT content is less than 0.80%, which would result from the excellent toughness of the CNT and/or the easier slip along the powder boundary. On the other hand, the fracture mode changes from the brittle fracture mode of the monolithic BAA characterized in vein-like pattern and smooth cleavage pattern (see Fig. 7(a)) to the complex fracture mode of the BAA composite characterized in brittle vein-like pattern and ductile dimple-like pattern (see Fig. 7(b)). However, the modulus and strain limit of the BAA composites sharply decrease when the CNT exceeds 0.80%. It would result from that the strength of the powder interface is obviously influenced by the serious oxidization and the excessive CNT addition. It is clearly seen from Fig. 7(c) that the compacts fracture along with the powder boundary, and the powders are not seriously deformed in the consolidation procedure.

5 Conclusions

1) The density and the compression strength of the consolidated specimens decrease with increasing CNT content.

2) The thermal conductivity of the compacts decreases when the CNT content is less than 0.10% and exceeds 0.60%, respectively, while increases when the CNT content is between 0.10% and 0.60%.

3) The strain limit and the modulus of the compacts are obviously improved when the CNT content is less than 1.00%, while decrease significantly when the CNT content exceeds 1.00%.

4) The optimum CNT addition is less than 0.20% at the comprehensive properties point of view.

References

[1] WANG W H, DONG C, SHEK C H. Bulk metallic glasses [J]. Mater Sci Eng R, 2004, 44: 45−89.

[2] LIU Y H, WANG G, WANG R J, ZHAO D Q, PAN M X, WANG W H. Super plastic bulk metallic glasses at room temperature [J]. Science, 2007, 315: 1385−1388.

[3] KIM Y C, NA J H, PARK J M, KIM D H, LEE J K, KIM W T. Role of nanometer-scale quasicrystals in improving the mechanical behavior of Ti-based bulk metallic glasses [J]. Appl Phys Lett, 2003, 83: 3093−3095.

[4] BAE D H, LEE M H, KIM D H, SORDELET D J. Plasticity in $Ni_{59}Zr_{20}Ti_{16}Si_2Sn_3$ metallic glass matrix composites containing brass fibers synthesized by warm extrusion of powders [J]. Appl Phys Lett, 2003, 83: 2312−2314.

[5] LEE J K, KIM H J, KIM T S, KIM Y C, BAE J C. Consolidation behavior of Cu- and Ni-based bulk metallic glass composites [J]. J Alloys Compd, 2007, 434−435: 336−339.

[6] SON C Y, LEE S B, LEE S K, KIM C P, LEE S. Correlation of microstructure and compressive properties of amorphous matrix composites reinforced with tungsten continuous fibers or porous foams [J]. Mater Sci Eng A, 2010, 527: 4028−4034.

[7] AHN J H, KIM Y J, KIM B K. Ni−Zr−Ti−Si−Sn/Cu metallic glass composites prepared by magnetic compaction [J]. Mater Lett, 2006, 60: 3747−3751.

[8] XIE G Q, ZHANG W, LOUZGINE-LUZGIN D V, KIMURA H, INOUE A. Fabrication of porous Zr−Cu−Al−Ni bulk metallic glass by spark plasma sintering process [J]. Scripta Mater, 2006, 55: 687−690.

[9] KIM T S, LEE S Y, LEE J K, KIM H J, KIM D H, BAE J C. Microstructure control of Cu-base metallic glass powder composites by extrusion [J]. Mater Sci Eng A, 2007, 449−451: 880−883.

[10] DEMETRIOU M D, DUAN G, VEAZEY C, BLAUWE K D, JOHNSON W L. Amorphous Fe-based metal foam [J]. Scripta Mater, 2007, 57: 9−12.

[11] LU Z P, MA D, LIU C T, CHANG Y A. Competitive formation of glasses and glass–matrix composites [J]. Intermetallics, 2007, 15: 253−259.

[12] HUI X, DONG W, CHEN G L, YAO K F. Formation, microstructure and properties of long-period order structure reinforced Mg-based bulk metallic glass composites [J]. Acta Mater, 2007, 55: 907−920.

[13] JIANG F, ZHANG D H, ZHANG L C, ZHANG Z B, HE L, SUN J, ZHANG Z F. Microstructure evolution and mechanical properties of $Cu_{46}Zr_{47}Al_7$ bulk metallic glass composite containing CuZr

crystallizing phases [J]. Mater Sci Eng A, 2007, 467: 139−145.
[14] WADA T, WANG X M, KIMURA H, INOUE A. Preparation of a Zr-based bulk glassy alloy foam [J]. Scripta Mater, 2008, 59: 1071−1074.
[15] BROTHERS A H, PRINE D W, DUNAND D C. Acoustic emissions analysis of damage in amorphous and crystalline metal foams [J]. Intermetallics, 2006, 14: 857−865.
[16] BIAN Z, WANG R J, ZHAO D Q, PAN M X. Excellent ultrasonic absorption ability of carbon-nanotube-reinforced bulk metallic glass composites [J]. Appl Phys Lett, 2003, 82: 2790−2793.
[17] BIAN Z, WANG R J, WANG W H. Carbon-nanotube-reinforced Zr-based bulk metallic glass composites and their properties [J]. Adv Funct Mater, 2004, 14: 55−63.
[18] LEE J K, LEE K B, LEE M H, KIM T S, BAE J C. Microstructure and mechanical properties of metallic glass/metallic glass composites [J]. J Alloys Compd, 2009, 483: 286−288.
[19] KIM Y B, PARK H M. Synthesis of amorphous/crystalline composite using electroless copper plated amorphous powder [J]. Mater Sci Eng A, 2005, 396: 166−171.
[20] VENKATARAMAN S, ECKERT J, SCHULTZ L, SORDELET D J. Studies on the crystallization kinetics of Cu-reinforced partially crystalline $Cu_{47}Ti_{33}Zr_{11}Ni_8Si_1$ metallic glass composite [J]. J Alloys Compd, 2007, 434−435: 203−206.
[21] KIM C K, LEE H S, SHIN S Y, LEE J C, KIM D H, LEE S. Microstructure and mechanical properties of Cu-based bulk amorphous alloy billets fabricated by spark plasma sintering [J]. Mater Sci Eng A, 2005, 406: 293−299.
[22] AN W K, CAI A H, XIONG X, LIU Y, LUO Y, LI T L, LI X S. Thermal, mechanical and corrosive behaviors of a Cu-based metallic glass [J]. Adv Mater Res, 2011, 146−147: 1491−1497.
[23] CAI A H, AN W K, LI X S, LUO Y, LI T L. Propery of Cu−Zr−Ti ternary alloys [J]. Adv Mater Res, 2011, 146−147: 1477−1481.
[24] SOMEKAWA H, INOUE A, HIGASHI K. Superplastic and diffusion bonding behavior on Zr−Al−Ni−Cu metallic glass in supercooled liquid region [J]. Scripta Mater, 2004, 50: 1395−1399.
[25] SWISTON A J, HUFNAGEL T C, WEIHS T P. Joining bulk metallic glass using reactive multilayer foils [J]. Scripta Mater, 2003, 48: 1575−1580.
[26] HARMS U, SHEN T D, SCHWARZ R B. Thermal conductivity of $Pd_{40}Ni_{40-x}Cu_xP_{20}$ metallic glasses [J]. Scripta Mater, 2002, 47: 411−414.
[27] CHOY C L, TONG K W, WONG H K, LEUNG W P. Thermal conductivity of amorphous alloys above room temperature [J]. J Appl Phys, 1991, 70: 4919−4925.
[28] YAMASAKI M, KAGAO S, KAWAMURA Y. Thermal diffusivity and conductivity of $Zr_{55}Al_{10}Ni_5Cu_{30}$ bulk metallic glass [J]. Scripta Mater, 2005, 53: 63−67.
[29] TIAN Y, LI Z Q, JIANG E Y. Low temperature specific heat and thermal conductivity of bulk metallic glass $(Cu_{50}Zr_{50})_{94}Al_6$ [J]. Solid State Comm, 2009, 149: 1527−1530.
[30] CHO Y, CHOI G, KIM D. A method to fabricate field emission tip arrays by electrocodeposition of single-wall carbon nanotubes and nickel [J]. Electrochem Solid-State Lett, 2006, 9: G107−110.
[31] PESETSKI A A, BAUMGARDNER J E, KRISHNASWAMY S V, ZHANG H, ADAM J D, KOCABAS C, BANKS T, ROGERS J A. A 500 MHz carbon nanotube transistor oscillator [J]. Appl Phys Lett, 2008, 93: 123506-1−2.
[32] de HEER W A, CHÂTELAIN A, UGARTE D. A carbon nanotube field-emission electron source [J]. Science, 1995, 270: 1179−1180.
[33] ZHU W, BOWER C, ZHOU O, KOCHANSKI G, JIN S. Large current density from carbon nanotube field emitters [J]. Appl Phys Lett, 1999, 75: 873−875.
[34] YANG Y L, WANG Y D, REN Y, HE C S, DENG J N, NAN J, CHEN J G, ZUO L. Single-walled carbon nanotube-reinforced copper composite coatings prepared by electrodeposition under ultrasonic field [J]. Mater Lett, 2008, 62: 47−50.
[35] LIANG G D, BAO S P, TJONG S C. Microstructure and properties of polypropylene composites filled with silver and carbon nanotube nanoparticles prepared by melt-compounding [J]. Mater Sci Eng B, 2007, 142: 55−61.
[36] XIANG C S, PAN Y B, GUO J K. Electromagnetic interference shielding effectiveness of multiwalled carbon nanotube reinforced fused silica composites [J]. Ceramics Inter, 2007, 33: 1293−1297.
[37] LI G Y, WANG P M, ZHAO X H. Pressure-sensitive properties and microstructure of carbon nanotube reinforced cement composites [J]. Cement Concrete Comp, 2007, 29: 377−382.
[38] HSU C F, LIN H M, LEE P Y. Characterization of mechanically alloyed Ti-based bulk metallic glass composites containing carbon nanotubes [J]. Adv Eng Mater, 2008, 10: 1053−1055.

一种碳纳米管增强的铜基块体非晶合金复合材料

蔡安辉[1,2]，熊 翔[2]，刘 咏[2]，安伟科[1]，周果君[1]，罗 云[1]，李铁林[1]，李小松[1]

1. 湖南理工学院 机械工程学院，岳阳 414006；
2. 中南大学 粉末冶金国家重点实验室，长沙 410083

摘 要：采用热压成型法制备碳纳米管增强的 $Cu_{50}Zr_{40}Ti_{10}$ 非晶合金复合材料，并研究碳纳米管添加量对其密度、热导率和力学性能的影响。结果发现，随着碳纳米管含量的增加，块体非晶合金复合材料的密度和抗压强度都降低；当碳纳米管的含量少于 0.1%或超过 0.6%时，块体非晶合金复合材料的热导率随着碳纳米管含量的增加而降低，然而，当碳纳米管的含量介于 0.1%和 0.6%之间时，块体非晶合金复合材料的热导率随着碳纳米管含量的增多而增大；当碳纳米管的含量少于 1.0%时，块体非晶合金复合材料的应变量与模量明显得到提高，并随着碳纳米管含量的进一步增加块体非晶合金复合材料的应变量与模量明显下降。综合各种性能得出，碳纳米管的添加量少于 0.2%为宜。

关键词：Cu 基非晶合金；碳纳米管；复合材料

(Edited by YANG Hua)